Mechanical Systems and Signal Processing 162 (2022) 108062

Contents lists available at ScienceDirect

Mechanical Systems and Signal Processing

journal homepage: www.elsevier.com/locate/ymssp

Dynamics estimator based robust fault-tolerant control for VTOL UAVs trajectory tracking

Kewei Xia, Wonmo Chung, Hungsun Son *

Department of Mechanical Engineering, Ulsan National Institute of Science and Technology, Ulsan 44919, Republic of Korea

ARTICLE INFO

Keywords:
VTOL Unmanned aerial vehicles
Robust control
Fault-tolerant
Trajectory tracking
Non-singularity

ABSTRACT

This paper investigates the control issue of the trajectory tracking of vertical take-off and landing (VTOL) unmanned aerial vehicles (UAVs) in the presence of partial propeller fault and external disturbance. In particular, a robust passive fault-tolerant control strategy is proposed by introducing a first-order filter based dynamics estimator. First, a bounded force command is exploited by employing a new smooth saturation function in the output of the estimator. A sufficient condition in terms of a specified parameter selection criteria is provided to ensure the non-singularity extraction of the command attitude. Then, a torque command is applied to the attitude loop tracking. Since there is merely one filter parameter involved in the dynamics estimator, the practical implementation and parameter tuning can be significantly simplified. Stability analysis indicates that the proposed control strategy guarantees the semi-globally ultimately bounded tracking of VTOL UAVs subject to partial propeller fault and external disturbance. Simulation and experiment results with comparison examples are performed to validate the effectiveness of the proposed strategy. Experimental results show that the proposed strategy achieves the trajectory tracking with a good performance (mean deviation 0.0074 m and standard deviation 0.1202 m) in the presence of 35% propeller fault and 4 m/s persistent wind disturbance.

1. Introduction

Vertical take-off and landing (VTOL) unmanned aerial vehicle (UAV), as a core tool in many military and civil applications, has been widely studied in recent decades due to its excellent capabilities like unmanned operation, rapid maneuverability and agile maneuverability [1,2]. Typical applications include military surveillance and attack, reconnaissance operation, forest fires prevention, etc [3]. In possession of the under-actuated structure, VTOL UAV is relatively sensitive to external disturbance and internal uncertainty [4]. Therefore, the control development with high reliability and robustness for VTOL UAV trajectory tracking is considerably significant but challenging.

To achieve the trajectory tracking of VTOL UAVs, varieties of control algorithms have been addressed. A thrust constrained controller [5] and a neural network based adaptive approach [6] were designed for the model-scaled helicopter tracking, respectively. Adaptive control strategies were developed for the quadrotor tracking [7–9]. However, it is not always realistic that the UAV is operated without disturbance [5] or with constant disturbance [9]. A robust control strategy was proposed for the quadrotor tracking by using a three-loop design structure [10]. By combining a disturbance observer and an extended state observer, a robust controller

* Corresponding author.
E-mail addresses: kwxia134@gmail.com (K. Xia), momone@unist.ac.kr (W. Chung), hson@unist.ac.kr (H. Son).

https://doi.org/10.1016/j.ymssp.2021.108062
Received 7 October 2020; Received in revised form 10 May 2021; Accepted 14 May 2021
Available online 31 May 2021

was designed for the quadrotor tracking [11]. To improve the tracking performance, sigmoid tracking differentiator and extended state observer were introduced in the backstepping controller for the quadrotor system [12]. A model based robust control strategy was designed to achieve the trajectory tracking of a small helicopter [13]. Besides, a fixed-time adaptive controller was developed for a helicopter to achieve the ship landing task [14]. However, the position loop controllers developed in [6]-[8]-[14] are designed without the consideration of the singularity issue that arises from the command attitude extraction [3,5].

Due to the component degradation, damages, etc, unexpected faults may occur to propellers assembled in VTOL UAVs [1]. Without the fault-tolerant mechanism, the tracking performance and the system stability could be degraded. As for the attitude-only control problem of multirotor UAVs, adaptive sliding mode [15] and supertwisting-based observer [16] were introduced in the fault-tolerant control algorithms. By considering the altitude-attitude tracking of quadrotors, adaptive fault-tolerant strategies were applied [17,18]. However, the trajectory tracking of VTOL UAV in possession of an under-actuated property which prevents the direct implementations of the controllers provided by [15–18]. For the sake of the high performance trajectory tracking of VTOL UAVs subject to actuator fault, varieties of control approaches [19–25] have been employed. For example, observer-based fault estimator [19], adaptive estimator [20], and high-gain observer-based estimator [21] were introduced to compensate for the fault signals, and incremental nonsingular terminal sliding mode [22] and neuroadaptive [23] control approaches were developed, respectively. However, the estimator parameters in [19,21] are chosen based on solving linear matrix inequalities or matrix differential equations which could not provide an intuitive selection. Since the controllers in [19–21] are active fault-tolerant mechanism, the fault detection and diagnosis algorithms are provided which could increase the online computing burden. Moreover, according to [24,25], the active fault-tolerant capability is guaranteed by a sensitive and rapid detection algorithm. Improper detection and diagnosis could fail to provide active fault-tolerant capability which could deteriorate the system performance when fault occurs. Besides, the control strategies in [22,23] are developed under the hierarchical structure but can not provide the singularity free property that arises from command attitude extraction. Despite of the fact that the singularity free trajectory tracking are achieved in [25,26], the fault is considered to be constant in [26] which can not be always maintained in practice, and the upper bound of the uncertainty is introduced as the robust compensation in [25] which could result in a larger control than that is required. Moreover, fault-tolerant controllers were developed for extreme conditions such as one totally failed rotor [27] and insufficient actuator resources [28]. Although the system stabilities may be still maintained, the trajectory tracking may not be achieved [27,28].

This paper addresses the control development for the trajectory tracking of VTOL UAVs with partial propeller fault and external disturbance. The dynamics estimator [29,30] in possession of a simple structure has been shown to be an effective way to compensate for the mechanical system uncertainty. Benefit from a single filter parameter, the practical implementation and parameter tuning could be simple and easy. To this end, the dynamics estimator is exploited for the compensation for the dynamics uncertainty. Based on the hierarchical development, a robust fault-tolerant strategy is proposed such that a force command and a torque command are applied in the position and attitude tracking, respectively. It is proved that the proposed control strategy ensures the ultimate boundedness of the tracking error. Experiment examples are conducted on a real quadrotor platform to validate the proposed strategy. The main contributions are summarized as follows.

1. In contrast to the control algorithms in [19–23] that are designed regardless of the singularity arising from the command attitude extraction, a bounded force command is proposed such that the non-singularity extraction is ensured by a specified parameter selection criteria. With such a control development, the system robustness in harsh environment can be enhanced.
2. Instead of the fault estimators provided by [19–21], a first-order filter based dynamics estimator is introduced as the compensation mechanism. A new saturation function is developed to ensure a differentiable property of the designed force command. Since only one filter parameter is involved in the estimator, the parameter tuning can be significantly reduced. This could contribute to a simple implementation in practical setup. Due to the passive fault-tolerant mechanism, the fault diagnosis development [19–21] can be also removed such that the online computing burden can be reduced.
3. In addition to the numerical simulation validations in [22–25], the proposed strategy is performed on a quadrotor UAV by real flight experiments in three different cases. Experimental results show that the nonsingular controller and PID controller fail to provide sufficient fault-tolerant capability for the completion of trajectory tracking in cases I and III, respectively, and that the proposed strategy can achieve the tracking in case II on the improvement of the mean derivation and standard derivation by 69.00% and 68.83% with merely 4.15% additional energy consumption, respectively, rather than the conventional PID controller.

The remaining sections are arranged as follows. The tracking problem to be solved is stated in Section 2. The control development is presented in Section 3. The closed-loop stability is analyzed in Section 4. Numerical simulations are provided in Section 5. Experimental results are performed and discussed in Section 6. Finally, the conclusions are summarized in Section 7.

Notations. $\mathbb{R}^{m\times n}$ denotes the $m \times n$ Euclidean space, $|\cdot|$ the absolute value of a scalar, and $\|\cdot\|$ the Euclidean norm of a vector. For a square matrix $X \in \mathbb{R}^{n\times n}$, $\bar{\lambda}(X)$ and $\underline{\lambda}(X)$ denote its minimum and maximum eigenvalues, respectively. For $x = [x_1, x_2, x_3]^T \in \mathbb{R}^3$, the superscript $\times$ is defined as $x^\times = [0, -x_3, x_2; x_3, 0, -x_1; -x_2, x_1, 0]$. For positive constants a and b, the smooth saturation function $\mathscr{F}_{a,b} \in \mathscr{C}$ is defined as

$$\mathscr{T}_{a,b}\left(x\right)=\begin{cases} a+b\left(1-e^{-\frac{1}{b}\left(x-a\right)}\right), & \text{if} x>a,\\ x, & \text{if}-a\leqslant x\leqslant a,\\ -a-b\left(1-e^{\frac{1}{b}\left(x+a\right)}\right), & \text{if} x<-a. \end{cases}$$

2. Problem formulation

2.1. Dynamics modelling

In terms of the Euler-Newton formula, the kinematics and dynamics of the VTOL UAV are given by

$$\dot{p}=v, \tag{1}$$

$$\dot{v}=-g\widehat{e}_3+\frac{T}{m}R\widehat{e}_3+\frac{d_t}{m}, \tag{2}$$

$$\dot{q}=\mathscr{P}(q)\omega, \tag{3}$$

$$J\dot{\omega}=-\omega^{\times}J\omega+\tau+d_\tau, \tag{4}$$

where $p\in\mathbb{R}^3$ is the position of the UAV with respect to the center of gravity expressed in the Earth-fixed inertial frame, $v\in\mathbb{R}^3$ is the velocity, g is the local gravitational acceleration, $\widehat{e}_3\triangleq[0,0,1]^T$, T is the applied thrust along $\widehat{e}_3$ expressed in the body-fixed frame, m is the mass, d_t is the external disturbance force, $q=[q_0,q_r^T]^T\in\mathbb{R}\times\mathbb{R}^3$ is the unit quaternion representing the attitude of the UAV, $\mathscr{P}\left(q\right)=\frac{1}{2}\left[-q_r^T;q_r^{\times}+q_0I_3\right]$, $\omega\in\mathbb{R}^3$ is the angular velocity, $J\in\mathbb{R}^{3\times3}$ is the inertial matrix, $\tau\in\mathbb{R}^3$ is the applied torque, $d_\tau\in\mathbb{R}^3$ is the disturbance torque, $R\in\mathrm{SO}(3)$ is the rotation matrix determined by [31]

$$R\triangleq R(q)=\left(q_0^2-q_r^Tq_r\right)I_3+2q_rq_r^T+2q_0q_r^{\times}. \tag{5}$$

Let $f_i(i=1,2,\cdots,N)$ be the thrust generated by each rotor which is formulated by the rotational speed of each propeller $f_i=k_\omega\omega_{ri}^2$, where k_ω is a positive parameter depending on multiple factors such as the air density and the geometric features of the blades, and ω_{ri} represents the rotational speed of each rotor. By considering the propeller fault, we have $f_i=(1-\upsilon_i)k_\omega\omega_{ri}^2$, where $0<\upsilon_i\leq1$ is the fault signal of each propeller which can be time-varying. Then, the force and torque commands subject to fault signals can be determined by

$$T=T_0-T_f,\tau=\tau_0-\tau_f. \tag{6}$$

where T_0 and τ_0 are the force and torque commands free from thruster faults, T_f and τ_f are the combined force and torque under faulty propellers.

Remark 1. In this paper, we formulate a generalized VTOL UAV model by 1–4 that could characterize a variate of multirotor UAVs like hexarotors, quadrotor, etc which are driven by the propellers. To exemplify, we consider a quadrotor subject to propeller fault. The faulty model (6) can be illustrated as follows: $T_0=\sum_{i=1}^4k_\omega\omega_{ri}^2$, $T_f=\sum_{i=1}^4\upsilon_ik_\omega\omega_{ri}^2$, $\tau_0=\left[lk_\omega(\omega_{r4}^2-\omega_{r2}^2),lk_\omega(\omega_{r1}^2-\omega_{r3}^2),Ck_\omega\sum_{i=1}^4(-1)^{i+1}\omega_{ri}^2\right]^T$, $\tau_f=\left[lk_\omega(\upsilon_4\omega_{r4}^2-\upsilon_2\omega_{r2}^2),lk_\omega(\upsilon_1\omega_{r1}^2-\upsilon_3\omega_{r3}^2),Ck_\omega\sum_{i=1}^4(-1)^{i+1}\upsilon_i\omega_{ri}^2\right]^T$, where l is the distance from the quadrotor c.g. to the rotation axis of each rotor and C is the anti-torque coefficient.

2.2. Control objective

Suppose that the full motion information of the VTOL UAV can be obtained by proper measurement devices. Consider the dynamics system 1–4, the control objective is to develop force command T_0 and torque command τ_0 in the presence of propeller fault (6) such that the UAV can track a desired reference trajectory. More specifically, given a reference trajectory p_0, the objective is to guarantee the ultimately bounded tracking with adjustable errors.

Assumption 1. The reference trajectory and its derivatives are all bounded. In particular, $\sup(\|\ddot{p}_0\|)\leqslant\overline{a}_0<g$, where $\overline{a}_0$ is a positive constant.

Assumption 2. The external disturbance and faulty signal, and their derivatives are all bounded. In particular, there exists a positive constant $\overline{u}$ satisfying $\overline{u}<g-\overline{a}_0$ such that $\left\|d_t/m-T_fR_c\widehat{e}_3/m\right\|\leqslant\overline{u}$.

Remark 2. Assumption 1 is commonly used to ensure the trajectory tracking of VTOL UAVs solvable. The boundedness of T_f can be

guaranteed if the designed force command T is naturally bounded, and a differentiable T could ensure a uniformly continuous T_f. As a trajectory tracking problem, Assumption 2 provides the controllability and fault recoverability of the VTOL UAV system [25,26]. Therefore, $\bar{u}$ can be determined by considering both the robust performance to the external disturbance and expected fault-tolerant capability (for example, total 30% loss of efficiency). This implies that the trajectory tracking may not be achieved if the propellers can not generate sufficient control energy. However, the occurrence of too serious fault (for example, one or two rotors totally failed) does not imply that the UAV is not controllable [27,28]. At the expense of yaw control, the position system may be still stabilized rather than tracking. In this paper, only the trajectory tracking issue is investigated.

3. Control strategy development

In this section, we present a robust fault-tolerant control strategy for the trajectory tracking of the VTOL UAV. In particular, by introducing a dynamics estimator [29,30], a bounded force command and a torque command are developed for the position and attitude loops tracking, respectively.

3.1. Force command development

Define $\tilde{p} = p - p_0$ and $\tilde{v} = v - \dot{p}_0$ as the position and velocity tracking error, respectively. By recalling (1), (2) and (6), we have

$$\dot{\tilde{p}} = \tilde{v}, \tag{7}$$

$$\dot{\tilde{v}} = -g\hat{e}_3 - \ddot{p}_0 + u_0 + u_u + \frac{T_0 - T_f}{m}\left(R - R_c\right)\hat{e}_3, \tag{8}$$

where $u_0 = T_0 R_c \hat{e}_3/m = [u_{0x}, u_{0y}, u_{0z}]^T$ is the force command, R_c is the command rotation matrix and $u_u = d_t/m - T_f R_c \hat{e}_3/m$. According to [2], the system 7–8 can be treated as its nominal system

$$\dot{\tilde{p}} = \tilde{v}, \tag{9}$$

$$\dot{\tilde{v}} = -g\hat{e}_3 - \ddot{p}_0 + u_0 + u_u, \tag{10}$$

perturbed by $(T_0 - T_f)(R - R_c)\hat{e}_3/m$, and $R \to R_c$ and $T_0 \in \mathscr{L}_\infty$ is sufficient to ensure $(T_0 - T_f)(R - R_c)\hat{e}_3/m \to 0$. Define a variable $z = \tilde{v} + K_1\tilde{p}$, where $K_1 = \mathrm{diag}(\kappa_{1x}, \kappa_{1y}, \kappa_{1z})$ is a positive definite matrix. Design the following force command

$$u_0 = g\hat{e}_3 + \ddot{p}_0 - \frac{K_2 z}{\sqrt{1 + z^T z}} - \frac{K_2 \tilde{v}}{\sqrt{1 + \tilde{v}^T \tilde{v}}} - \mathscr{F}\left(\hat{u}_u\right), \tag{11}$$

where $K_2 = \mathrm{diag}(\kappa_{2x}, \kappa_{2y}, \kappa_{2z})$ is a positive definite matrix with $\kappa_{2i}, i = x, y, z$ being positive constants, $\mathscr{F}(\hat{u}_u) \triangleq \mathscr{F}_{\bar{u},\Delta\bar{u}}(\hat{u}_u) = [\mathscr{F}_{\bar{u},\Delta\bar{u}}(\hat{u}_{u1}), \mathscr{F}_{\bar{u},\Delta\bar{u}}(\hat{u}_{u2}), \mathscr{F}_{\bar{u},\Delta\bar{u}}(\hat{u}_{u3})]^T$, $\Delta\bar{u}$ is a small positive constant. Moreover, $\hat{u}_u = [\hat{u}_{u1}, \hat{u}_{u2}, \hat{u}_{u3}]^T$ is the output of the following dynamics estimator

$$\hat{u}_u = \frac{\tilde{v} - v_v}{\alpha_p} + v_u, \tag{12}$$

where $\alpha_p > 0$ is the filter parameter, v_v and v_u are the filtered signals by filtering $\tilde{v}$ and $g\hat{e}_3 + \ddot{p}_0 - u_0$ through the following first-order filters

$$\alpha_p \dot{v}_v + v_v = \tilde{v}, \tag{13}$$

$$\alpha_p \dot{v}_u + v_u = g\hat{e}_3 + \ddot{p}_0 - u_0, \tag{14}$$

with initial states $v_v(0) = 0$ and $v_u(0) = 0$. In view of $\|R_c\hat{e}_3\| = 1$, the applied thrust T_0 can be determined by

$$T_0 = m\|u_0\|. \tag{15}$$

Substituting (11) into (10), by defining $\tilde{u}_s = \mathscr{F}(\hat{u}_u) - u_u$, gives the following closed-loop position system

$$\dot{\tilde{v}} = -\frac{K_2 z}{\sqrt{1 + z^T z}} - \frac{K_2 \tilde{v}}{\sqrt{1 + \tilde{v}^T \tilde{v}}} - \tilde{u}_s. \tag{16}$$

3.2. Command attitude extraction

Based on the hierarchical framework, the command attitude $q_c = [q_{c0}, q_{cr}^T]^T \in \mathbb{R} \times \mathbb{R}^3$ is extracted from the force command u_0 [2]. A feasible extraction algorithm is shown as follows. If the command force u_0 is developed such that

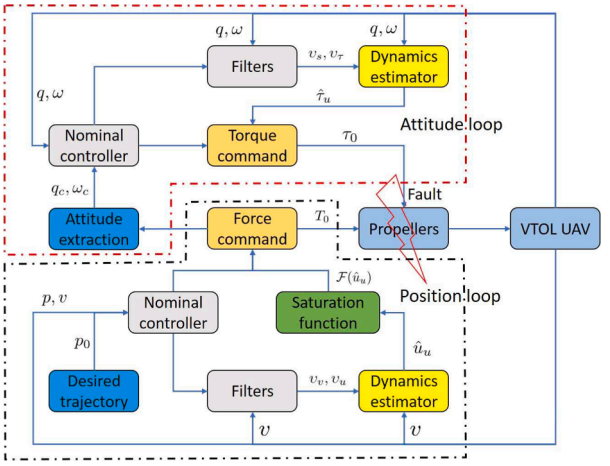

Fig. 1. Control flow diagram.

$$u_0 \neq \mathscr{U} \triangleq \left\{u \in \mathbb{R}^3 \middle| u = [0, 0, u_{0z}]^T, u_{0z} \leqslant 0\right\}, \tag{17}$$

the command quaternion q_c can be extracted as $q_{c0} = \sqrt{(1 + u_{0z}/\|u_0\|)/2}$ and $q_{cr} = [-u_{0y}, u_{0x}, 0]^T/(2\|u_0\|q_{c0})$.

Proposition 1. The attitude extraction is singularity free if the control parameter κ_{2z} is chosen as $\kappa_{2z} < (g - \overline{a}_0 - \overline{u} - \Delta\overline{u})/2$.

Proof. In view of the fact that $|z_z|/\sqrt{1 + z^T z} < 1$ and $|\widetilde{\nu}_z|/\sqrt{1 + \widetilde{\nu}^T\widetilde{\nu}} < 1$, it follows from (11) that

$$u_{0z} > g - \overline{a}_0 - \overline{u} - \Delta\overline{u} - 2\kappa_{2z} > 0. \tag{18}$$

This ensures the nonsingular condition $u_0 \neq \mathscr{U}$ in (17). In addition, recalling (11) gives that

$$T_0 = m\left\|u_0\right\| \leqslant \overline{T} \triangleq m\left(g + \sqrt{3}\left(\overline{a} + \overline{u} + \Delta\overline{u} + 2\overline{\lambda}\left(K_2\right)\right)\right). \tag{19}$$

It can be concluded that T_0 is naturally bounded. □

3.3. Torque command development

Since the command attitude has been obtained, we next show the torque command development for the attitude loop. Define $\widetilde{q} = [\widetilde{q}_0, \widetilde{q}_r^T]^T$ as the attitude error. According to [31], it can be derived by the quaternion product

$$\widetilde{q} = q_c^{-1} \odot q = \left[q_{c0}q_0 + q_{cr}^T q_r, \left(q_{c0}q_r - q_0 q_{cr} - q_{cr}^{\times} q_r\right)^T\right]^T, \tag{20}$$

where operator $\odot$ is the quaternion product, and $q_c^{-1} = [q_{c0}, -q_{cr}^T]^T$. According to [31], its kinematics satisfies

$$\dot{\widetilde{q}} = \mathscr{P}\left(\widetilde{q}\right)\widetilde{\omega}, \tag{21}$$

where $\widetilde{\omega} = \omega - \widetilde{R}^T\omega_c$ is the error angular velocity, $\widetilde{R} = R(\widetilde{q}), \omega_c = 4\mathscr{P}(q_c)^T\dot{q}_c$ is the command angular velocity. To avoid the complicated computing of $\dot{q}_c$, a command filter [32] is employed. In terms of (4) and (6), the attitude error dynamics is derived as

$$J\dot{\widetilde{\omega}} = -\omega^{\times}J\omega + \tau_0 - \tau_f + d_\tau + J\left(\widetilde{\omega}^{\times}\widetilde{R}^T\omega_c - \widetilde{R}^T\dot{\omega}_c\right). \tag{22}$$

Introduce a variable $s = \widetilde{\omega} + \kappa_3\widetilde{q}_r$. Taking its derivative gives

$$J\dot{s} = -\omega^{\times}J\omega + \tau_0 - \tau_f + d_\tau + J\left(\widetilde{\omega}^{\times}\widetilde{R}^T\omega_c - \widetilde{R}^T\dot{\omega}_c\right) + \frac{\kappa_3}{2}\left(\widetilde{q}_r^{\times} + \widetilde{q}_0 I_3\right)\widetilde{\omega} = \varrho_r + \tau_0 + \tau_u, \tag{23}$$

where $\varrho_r = -\omega^{\times}J\omega + J\widetilde{\omega}^{\times}\widetilde{R}^T\omega_c + \kappa_3(\widetilde{q}_r^{\times} + \widetilde{q}_0 I_3)\widetilde{\omega}/2$, and $\tau_u = d_\tau - \tau_f - J\widetilde{R}^T\dot{\omega}_c$. We design the following torque command

$$\tau_0 = -\widetilde{q}_r - \kappa_4 s - \varrho_r - \widehat{\tau}_u, \tag{24}$$

where κ_4 is a positive constant. Besides, $\widehat{\tau}_u$ is the output of the dynamics estimator

$$\widehat{\tau}_u = \frac{Js - \upsilon_s}{\alpha_a} + \upsilon_\tau, \tag{25}$$

where $\alpha_a > 0$ is the filter parameter, υ_s and υ_τ are filtered signals generated by

$$\alpha_a \dot{\upsilon}_s + \upsilon_s = Js, \tag{26}$$

$$\alpha_a \dot{\upsilon}_\tau + \upsilon_\tau = -\varrho_r - \tau_0, \tag{27}$$

with initial states being chosen as $\upsilon_z(0) = 0$ and $\upsilon_\tau(0) = 0$. Define the estimate error $\widetilde{\tau}_u = \widehat{\tau}_u - \tau_u$. By substituting the torque command (24) into (23), we have

$$J\dot{s} = -\widetilde{q}_r - \kappa_4 s - \widetilde{\tau}_u. \tag{28}$$

To facilitate the implementation of the proposed control strategy for the quadrotor trajectory tracking, a flow diagram is shown in Fig. 1.

4. Stability analysis

In this section, the overall closed-loop stability is analyzed. First, two propositions summarize the stability of the attitude-loop and position-loop tracking, respectively. Then, a theorem presents the main result of this paper.

Proposition 2. If the control parameters are chosen such that $\kappa_4 > \delta_a \alpha_a, \forall \delta_a > 0$, the closed-loop attitude error system (28) is ultimately bounded.

Proof. In terms of the design procedure of the dynamics estimator, $\widehat{\tau}_u$ can be regarded as the filtered version of the unknown function τ_u given by $\alpha_a \dot{\widehat{\tau}}_u + \widehat{\tau}_u = \tau_u$. Taking the derivative of $\widetilde{\tau}_u$ yields

$$\dot{\widetilde{\tau}}_u = \dot{\widehat{\tau}}_u - \dot{\tau}_u = -\frac{\widehat{\tau}_u - \tau_u}{\alpha_a} - \dot{\tau}_u = -\frac{1}{\alpha_a}\widetilde{\tau}_u - \dot{\tau}_u. \tag{29}$$

Choose the following Lyapunov function candidate

$$V_r = (1 - \widetilde{q}_0)^2 + \widetilde{q}_r^T \widetilde{q}_r + \frac{1}{2} s^T J s + \frac{1}{2\delta_a} \widetilde{\tau}_u^T \widetilde{\tau}_u. \tag{30}$$

Taking its derivative along the closed-loop trajectory (28), together with (21) and (29), yields

$$\dot{V}_r = \widetilde{q}_r^T \left(s - \kappa_3 \widetilde{q}_r \right) + s^T \left(-\widetilde{q}_r - \kappa_4 s - \widetilde{\tau}_u \right) + \frac{1}{\delta_a} \widetilde{\tau}_u^T \dot{\widetilde{\tau}}_u = -\kappa_3 \widetilde{q}_r^T \widetilde{q}_r - \kappa_4 s^T s - s^T \widetilde{\tau}_u - \frac{1}{\delta_a \alpha_a} \widetilde{\tau}_u^T \widetilde{\tau}_u - \frac{1}{\delta_a} \widetilde{\tau}_u^T \dot{\tau}_u \leqslant -\kappa_3 \widetilde{q}_r^T \widetilde{q}_r - \frac{\kappa_4}{2} s^T s - \left(\frac{1}{2\delta_a \alpha_a} - \frac{1}{2\kappa_4} \right) \widetilde{\tau}_u^T \widetilde{\tau}_u + \frac{\alpha_a \sigma_r^2}{2\delta_a}, \tag{31}$$

where $\sigma_r > 0$ is an unknown constant satisfying $\sup(\|\dot{\tau}_u\|) \leqslant \sigma_r$, $-s^T \widetilde{\tau}_u \leqslant \kappa_4 s^T s/2 + \widetilde{\tau}_u^T \widetilde{\tau}_u/(2\kappa_4)$ and $-\widetilde{\tau}_u^T \dot{\tau}_u \leqslant \widetilde{\tau}_u^T \widetilde{\tau}_u/(2\alpha_a) + \alpha_a \dot{\tau}_u^T \dot{\tau}_u/2$ are used. Define $\lambda_r = 1/(2\delta_a \alpha_a) - 1/(2\kappa_4)$. It follows from $\kappa_4 > \delta_a \alpha_a$ that $\lambda_r > 0$. Then, (31) can be derived as

$$\dot{V}_r \leqslant -\kappa_3 \widetilde{q}_r^T \widetilde{q}_r - \frac{\kappa_4}{2} s^T s - \frac{\lambda_r}{2} \widetilde{\tau}_u^T \widetilde{\tau}_u + \frac{\alpha_a \sigma_r^2}{2\delta_a}. \tag{32}$$

Let $\xi = [\widetilde{q}_r^T, s^T, \widetilde{\tau}_u^T]^T$. It follows that

$$\dot{V}_r \leqslant -k_r \left\| \xi \right\|^2 + \frac{\alpha_a \sigma_r^2}{2\delta_a}, \tag{33}$$

where $k_r = \min(\kappa_3, \kappa_4/2, \lambda_r/2)$. It can be concluded that $\dot{V}_r \leqslant 0$ if ξ is outside of the set $\mathscr{D}_\xi = \{\xi \left| \left\| \xi \right\| \leqslant \sigma_r \sqrt{\alpha_a/(2\delta_a k_r)} \right.\}$. Thus, we have $V_r \in \mathscr{L}_\infty$[1] which further implies $\widetilde{q}_r, s, \widetilde{\tau}_u \in \mathscr{L}_\infty$. Finally, it can be concluded that $\widetilde{q}_r$ and $\widetilde{\omega}$ ultimately converge to the sets $\mathscr{D}_{\widetilde{q}_r} = \{\widetilde{q}_r \left| \left\| \widetilde{q}_r \right\| \leqslant \sigma_r \sqrt{\alpha_a/(2\delta_a k_r)} \right.\}$ and $\mathscr{D}_{\widetilde{\omega}} = \{\widetilde{\omega} \left| \left\| \widetilde{\omega} \right\| \leqslant (1 + \kappa_3)\sigma_r \sqrt{\alpha_a/(2\delta_a k_r)} \right.\}$, respectively.

Proposition 3. If the control parameters are chosen such that $\kappa_{2z} < (g - \overline{a}_0 - \overline{u} - \Delta\overline{u})/2$ and $\alpha_p < \gamma^2 \underline{\lambda}(\Gamma) \Big/ \left(2\eta^2 \delta_p\right), \forall \delta_p, \gamma > 0$, where $\Gamma = \begin{bmatrix} K_2 & K_2 \\ K_2 & K_1 + K_2 \end{bmatrix}$ and $\eta = \overline{\lambda}(I_3 + K_1 K_2^{-1})$, the closed-loop position error system (16) is ultimately bounded.

[1] $\mathscr{L}_\infty = \{f(t) | \text{esssup}_{t \in \mathbb{R}^+} \|f(t)\| < \infty\}$.

Proof. The boundedness of $\widetilde{u}_s$ is first shown. Define $\widetilde{u}_u = \widehat{u}_u - u_u$. Choose a Lyapunov function $V_u = \widetilde{u}_u^T\widetilde{u}_u/2$. Its derivative can be derived as

$$\dot{V}_u = \widetilde{u}_u^T\left(-\frac{1}{\alpha_p}\widetilde{u}_u - \dot{u}_u\right) \leqslant -\frac{1}{\alpha_p}V_u + \frac{\alpha_p}{2}\sigma_t^2, \tag{34}$$

where $\sigma_t \geqslant \sup(\|\dot{u}_u\|)$. It then follows that $\left\|\widetilde{u}_u(t)\right\| \leqslant \sqrt{(\left\|\widetilde{u}_u(0)\right\| - \alpha_p^2\sigma_t^2)e^{-t/\alpha_p} + \alpha_p^2\sigma_t^2}$. It can be concluded that $\widetilde{u}_u(t)$ exponentially converge to $\left\|\widetilde{u}_u\right\| \leqslant \alpha_p\sigma_t$. From the definitions of $\mathscr{F}(\widehat{u}_u)$, $\widetilde{u}_u$ and $\widetilde{u}_s$, we have $\mathscr{F}(\widehat{u}_{ui}) = \widehat{u}_{ui}$ when $-\overline{u} \leqslant \widehat{u}_{ui} \leqslant \overline{u}, i = 1,2,3$. It follows that $\widetilde{u}_{si} = \widetilde{u}_{ui}$. When $\widehat{u}_{ui} > \overline{u}$, we have $\mathscr{F}\left(\widehat{u}_{ui}\right) = \overline{u} + \Delta\overline{u}\left(1 - e^{-\frac{1}{\Delta\overline{u}}\left(\widehat{u}_{ui} - \overline{u}\right)}\right)$. Define a function $y(\widehat{u}_{ui}) = \widehat{u}_{ui} - \mathscr{F}(\widehat{u}_{ui})$. It follows that

$$\frac{\partial y(\widehat{u}_{ui})}{\partial \widehat{u}_{u1}} = 1 - e^{-\frac{1}{\Delta\overline{u}}\left(\widehat{u}_{ui} - \overline{u}\right)} > 0, \forall \widehat{u}_{ui} > \overline{u}. \tag{35}$$

This implies that $\widehat{u}_{ui} > \mathscr{F}(\widehat{u}_{ui}), \forall \widehat{u}_{ui} > \overline{u}$. It further follows that $\widetilde{u}_{ui} > \widetilde{u}_{si} > 0$. Based on the same analysis, we have $\widetilde{u}_{ui} < \widetilde{u}_{si} < 0$, $\forall \widehat{u}_{ui} < -\overline{u}$. By summary, it can be concluded that $|\widetilde{u}_{si}| \leqslant |\widetilde{u}_{ui}|$ for any $\widehat{u}_{ui}$. Therefore, we have that $\widetilde{u}_s$ is bounded by $\|\widetilde{u}_s\| \leqslant \|\widetilde{u}_u\|$.

Next, define an expected region of attraction as follows

$$\mathscr{A}_\zeta = \{\zeta | \|\zeta\| < \overline{\zeta}, \overline{\zeta} > 0\}, \tag{36}$$

where $\zeta = [z^T, \widetilde{v}^T]^T$. It is trivial to show that there exists a positive constant $\gamma \triangleq \gamma(\overline{\zeta})$ such that $\gamma \leqslant 1/\sqrt{1+\overline{\zeta}^2}$. This implies that $\gamma\left\|\zeta\right\| \leqslant \left\|\zeta\right\|/\sqrt{1+\zeta^T\zeta}$, for $\zeta \in \mathscr{A}_\zeta$. Choose a Lyapunov function candidate

$$V_t = \sum_{r=z,v}\left(\sqrt{1+r^Tr} - 1\right) + \frac{1}{2}\widetilde{v}^TK_1K_2^{-1}\widetilde{v} + \frac{1}{2\delta_p}\widetilde{u}_u^T\widetilde{u}_u. \tag{37}$$

It follows that V_t is upper bounded by

$$V_t \leqslant \frac{\eta}{2}\left\|\zeta\right\|^2 + \frac{1}{2\delta_p}\left\|\widetilde{u}_u\right\|^2. \tag{38}$$

Taking the derivative of (37) along the closed-loop trajectory (9), (16) and (34) gives

$$\begin{aligned}
\dot{V}_t = {} & \frac{z^T}{\sqrt{1+z^Tz}}\dot{z} + \left(\frac{\widetilde{v}}{\sqrt{1+\widetilde{v}^T\widetilde{v}}} + K_2^{-1}K_1\widetilde{v}\right)^T\dot{\widetilde{v}} + \frac{1}{\delta_p}\widetilde{u}_u^T\dot{\widetilde{u}}_u = \frac{z^TK_1}{\sqrt{1+z^Tz}}\widetilde{v} + \left(\frac{z}{\sqrt{1+z^Tz}} + \frac{\widetilde{v}}{\sqrt{1+\widetilde{v}^T\widetilde{v}}} + K_2^{-1}K_1\widetilde{v}\right)^T \times \left(-\frac{K_2z}{\sqrt{1+z^Tz}}\right. \\
& \left. - \frac{K_2\widetilde{v}}{\sqrt{1+\widetilde{v}^T\widetilde{v}}} - \widetilde{u}_s\right) + \frac{1}{\delta_p}\widetilde{u}_u^T\dot{\widetilde{u}}_u \leqslant \\
& - \left(\frac{z}{\sqrt{1+z^Tz}} + \frac{\widetilde{v}}{\sqrt{1+\widetilde{v}^T\widetilde{v}}}\right)^TK_2\left(\frac{z}{\sqrt{1+z^Tz}} + \frac{\widetilde{v}}{\sqrt{1+\widetilde{v}^T\widetilde{v}}}\right) \\
& - \left(\frac{z}{\sqrt{1+z^Tz}} + \frac{\widetilde{v}}{\sqrt{1+\widetilde{v}^T\widetilde{v}}} + K_2^{-1}K_1\widetilde{v}\right)^T\widetilde{u}_s - \frac{1}{\delta_p\alpha_p}\widetilde{u}_u^T\widetilde{u}_u - \frac{1}{\delta_p}\widetilde{u}_u^T\dot{u}_u \leqslant \\
& - \underline{\lambda}\left(\Gamma\right)\left\|\frac{\zeta}{\sqrt{1+\zeta^T\zeta}}\right\|^2 - \frac{1}{2\delta_p\alpha_p}\widetilde{u}_u^T\widetilde{u}_u + \sqrt{2}\eta\left\|\zeta\right\|\left\|\widetilde{u}_u\right\| + \frac{\alpha_p\sigma_t^2}{2\delta_p}.
\end{aligned} \tag{39}$$

In terms of $\sqrt{2}\eta\left\|\zeta\right\|\left\|\widetilde{u}_u\right\| \leqslant \underline{\lambda}\left(\Gamma\right)\gamma^2\left\|\zeta\right\|^2/2 + \eta^2\left\|\widetilde{u}_u\right\|^2/\left(\gamma^2\underline{\lambda}(\Gamma)\right)$, together with $\gamma\|\zeta\| \leqslant \|\zeta\|/\sqrt{1+\zeta^T\zeta}$, it follows that

$$\dot{V}_t \leqslant -\frac{\underline{\lambda}\left(\Gamma\right)\gamma^2}{2}\left\|\zeta\right\|^2 - \left(\frac{1}{2\delta_p\alpha_p} - \frac{\eta^2}{\gamma^2\underline{\lambda}\left(\Gamma\right)}\right)\left\|\widetilde{u}_u\right\|^2 + c, \tag{40}$$

where $c = \alpha_p\sigma_t^2/(2\delta_p)$. Define $\lambda_t = 1/\left(2\delta_p\alpha_p\right) - \eta^2/\left(\gamma^2\underline{\lambda}(\Gamma)\right)$, where $\lambda_t > 0$ given the fact that $\alpha_p < \gamma^2\underline{\lambda}(\Gamma)\Big/\left(2\eta^2\delta_p\right)$. In terms of (38), we further derive (40) as follows

$$\dot{V}_t \leqslant -\frac{\underline{\lambda}\left(\Gamma\right)\gamma^2}{2}\left\|\zeta\right\|^2 - \lambda_t\left\|\widetilde{u}_u\right\|^2 + c \leqslant -k_tV_t + c, \tag{41}$$

Table 1
Simulation: Fault Coefficient.

	$0 \leqslant t < 40s$	$40s \leqslant t < 100s$	$t \geqslant 100s$
v_1	0	0	0
v_2	0	0	0
v_3	0	35%	10%
v_4	0	0%	30%

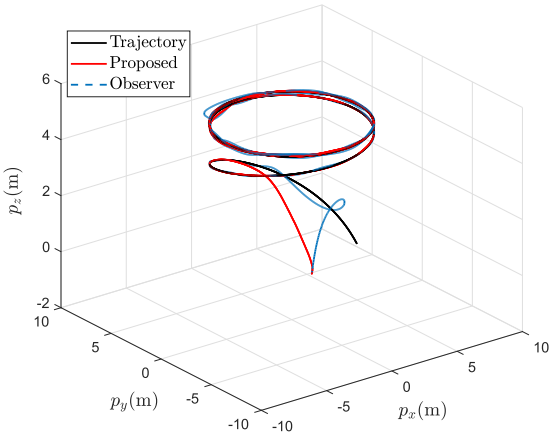

Fig. 2. Simulation: Trajectory of the UAV.

where $k_t = \min\left(\underline{\lambda}(\Gamma)\gamma^2, 2\lambda_t\right) \Big/ \max\left(\eta, 1/\delta_p\right)$. It follows that $V_t(t) \leqslant (V_t(0) - c/k_t)e^{-k_t t} + c/k_t$. It further follows that $\tilde{p}, \tilde{v}, \tilde{u}_u, \tilde{u}_s \in \mathscr{L}_\infty$. It can be concluded that V_t exponentially converges to the set $\mathscr{D}_{V_t} = \{V_t | V_t \leqslant c/k_t\}$. Next, it follows from (41) that $\dot{V}_t \leqslant 0$ if ζ is outside the set $\mathscr{D}_\zeta = \left\{\zeta \middle| \|\zeta\| \leqslant \sqrt{2c/\underline{\lambda}(\Gamma)}\right\}$. Thus, we know that ζ eventually converges to the set $\mathscr{D}_\zeta$. From the definitions of ζ and $z = \tilde{v} + K_1\tilde{p}$, we have that $\tilde{p}$ and $\tilde{v}$ ultimately converge to the sets $\mathscr{D}_{\tilde{p}} = \left\{\tilde{p} \middle| \|\tilde{p}\| \leqslant 2c/\left(\underline{\lambda}(\Gamma)\overline{\lambda}(K_1)^2\right)\right\}$ and $\mathscr{D}_{\tilde{v}} = \left\{\tilde{v} \middle| \|\tilde{v}\| \leqslant 2c/\left(\underline{\lambda}(\Gamma)\right)\right\}$, respectively.

□ Therefore, the main result can be summarized by following theorem.

Theorem 1. Consider the VTOL UAV dynamics expressed by 1–4. Suppose that Assumptions 1–2 hold. The proposed force command (11) and torque command (24) with dynamics estimators (25) and (12) guarantee that the ultimately bounded trajectory tracking is achieved.

Remark 3. In this paper, a dynamics estimator is employed to compensate for partial propeller fault and external disturbance simultaneously. This not only ensures high robustness to the control system but also provides simple parameter tuning and practical implementation. A novel smooth saturation function is introduced to provide a differentiable ability of the force command. Careful analysis indicates that sufficient small $\Delta\overline{u}$ could result in a high accuracy approximation to the standard saturation function. A larger $\overline{u}$ could provide a higher expected robust performance and fault recoverability. Nevertheless, a feasible compromise is inevitable with the non-singularity condition.

Remark 4. It is interesting to note that the selection of control parameters remains simple and intuitive despite of several parameters involved in the stability analysis. According to the design procedure, the parameters of the controller and estimator can be designed and tuned separately. From the definition of $\mathscr{D}_{\tilde{q}_r}$, it is trivial to show that larger κ_3 and κ_4 and smaller α_a could contribute to a smaller $\mathscr{D}_{\tilde{q}_r}$. In terms of $\underline{\lambda}(\Gamma)$, it can be also concluded that larger K_1 and K_2 and smaller α_p could contribute to a smaller $\mathscr{D}_{\tilde{p}}$. However, due to the selection criteria $\kappa_{2z} < (g - \overline{a}_0 - \overline{u} - \Delta\overline{u})/2, K_2$ can not be chosen arbitrarily large. $\mathscr{D}_{\tilde{p}}$ can be assigned arbitrarily small by merely increasing K_1. In practice, a suitable tradeoff among control requirements such as maximum control magnitude, environment disturbance, fault recoverability, etc, is also necessary.

5. Numerical simulations

In this section, numerical simulations are performed to show the effectiveness of the proposed strategy, where the disturbance observer [11,18,33] based control is also implemented in the same tracking scenario. To provide a fair comparison, both controllers are

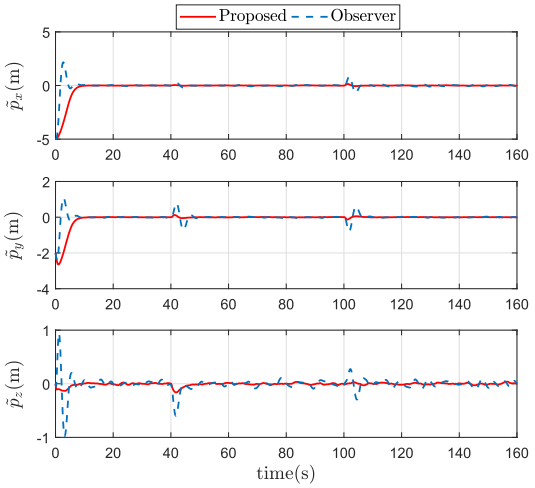

Fig. 3. Simulation: Tracking error.

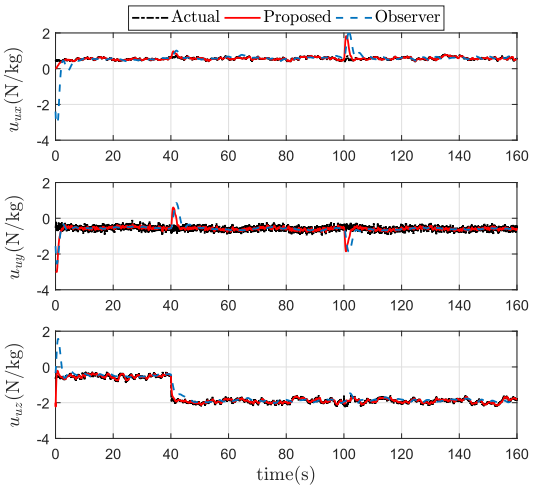

Fig. 4. Simulation: Estimation of system uncertainty.

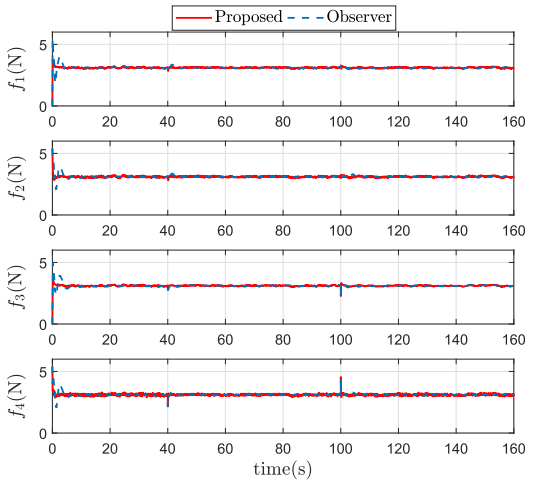

Fig. 5. Simulation: Actual control signal.

Table 2
Simulation: Tracking performance comparison.

Strategy	MD, m	SD, m	MT, s	EC, Ns
Proposed	1.3193×10^{-4}	0.0255	2.1616×10^{-4}	10.9094
Observer	7.0984×10^{-4}	0.1375	2.1712×10^{-4}	10.9161

Table 4
Tracking performance comparison.

Strategy	MD, m	SD, m	CT, s	EC, Ns
Proposed	0.0060	0.1004	3	7.2922
PID	0.0194	0.3222	8	7.0009

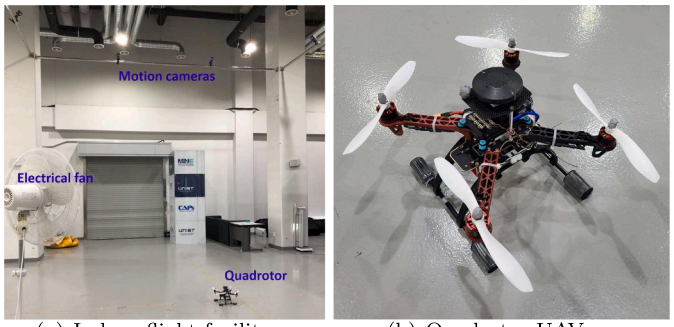

(a) Indoor flight facility. (b) Quadrotor UAV.

Fig. 6. Experiment setup.

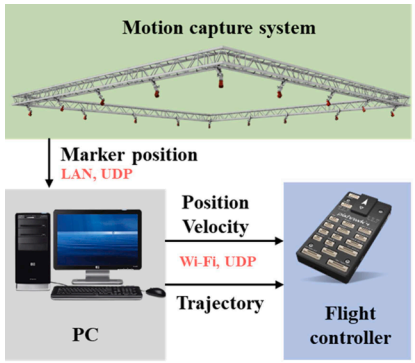

Fig. 7. Experiment workflow.

tuned well based on the same control energy cost. The system parameters of the quadrotor UAV are set as $m = 1.045\text{kg}$ and $J = \text{diag}(0.0064, 0.0064, 0.0128)\text{kgm}^2$. The reference trajectory is chosen as $p_0 = [5\cos(0.2t), 5\sin(0.2t), 5(1 - e^{-0.1t})]^T\text{m}$. The system states are initialized as $p(0) = [0, -2, 0]^T\text{m}$ and $\gamma(0) = [20, 0, 0]^T\text{deg}$. The initial states of the estimator and observer are all zero. The wind disturbance is injected in the simulation and its model can be found in our previous work [34]. The fault signals of the rotors are shown in Table 1. The control parameters of the proposed strategy are chosen as $\kappa_1 = \kappa_2 = 0.8, \kappa_3 = \kappa_4 = 0.4, \alpha_p = 0.25$ and $\alpha_a = 0.25$, and the observer based control (labeled by 'Observer') are $\kappa_1 = \kappa_2 = 0.8, \kappa_3 = \kappa_4 = 0.4, L_p = 0.6$ and $L_a = 2$. Simulation results are presented in Figs. 2–5.

Fig. 2 presents the trajectory of the UAV driven by each controller. Fig. 3 shows the time history of the tracking error in each direction. Fig. 4 provides the estimations of both algorithms. Fig. 5 collects the actual control signals. It can be observed that the proposed strategy ensures a better tracking performance with the same energy cost and that the dynamics estimator provides a faster response and higher accuracy. Table 2 summarizes the control performance of each strategy, where the mean deviation (MD) and standard deviation (SD) of the steady state are calculated from 10s, the mean time (MT) is the average computational time in each control step, and the energy consumption (EC) index is calculated by using $\sum_{i=1}^{4} \int_0^T f_i(t)\text{d}t/T$. It can be seen from Table 2 that the

Table 3
Fault Coefficient.

	$0 \leqslant t < 10$s	10s$\leqslant t < 20$s	$t \geqslant 20$s
υ_1	0	0	30%
υ_2	0	0	0
υ_3	0	10%	0
υ_4	0	15%	0

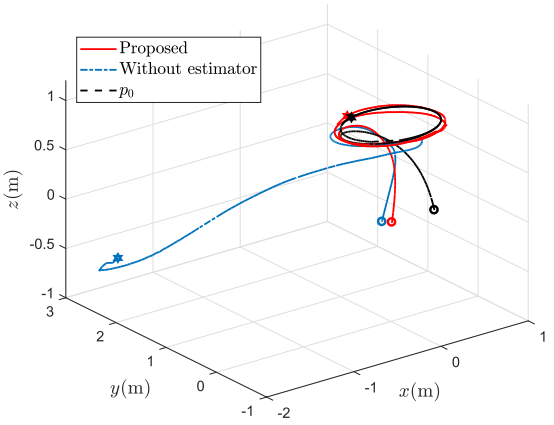

Fig. 8. Trajectory of quadrotor in CaseI. (∘ represents the initial position and * represents the final position.).

proposed control shows a better performance with higher accuracy. Besides, compared with the measurement and sensing frequency (attitude loop 200 Hz and position loop 120 Hz) in the experiment, the computational time of the proposed control can be neglected. (see Table 4).

6. Experimental validations

To validate the effectiveness of the proposed control strategy, experimental examples under different conditions are conducted on a quadrotor UAV platform which consists of an F330 DJI quadrotor, a motion capture system and the control center PC (refer to Fig. 6). The model parameters of the quadrotor are $m = 1.045\text{kg}$, $J = \text{diag}(0.0064,\ 0.0064,\ 0.0128)\text{kgm}^2$, $l = 0.225\text{m}$, and $C = 0.083\text{Nms}^2/\text{rad}^2$. The maximum output of each propeller is 5.4N. The attitude and angular velocity are measured by using an onboard inertial measurement unit (IMU) module, and the position and linear velocity are obtained by the motion capture system. The attitude-loop and position-loop are operated at 200 Hz and 120 Hz, respectively, where the Pixhawk provides the onboard flight control computer. Fig. 7 formulates the workflow of the experiment.

6.1. Parameter tuning

Before move on, the parameter tuning procedure of the proposed control strategy on real flight experiment is given. According to the separation principle, the controller and dynamics estimator parameters can be chosen individually. Based on the linearized model of the attitude-loop system around equilibrium $\widetilde{q}_r = \widetilde{\omega} = 0$, the nominal closed-loop can be approximately [33] derived as

$$2J\ddot{\widetilde{q}}_r = -\left(1+\kappa_3\kappa_4\right)\widetilde{q}_r - \left(2\kappa_4 + J\kappa_3\right)\dot{\widetilde{q}}_r, \tag{42}$$

where $\widetilde{\omega} \approx 2\dot{\widetilde{q}}_r$ is used. Its characteristic polynominal is given by

$$2J_i s_i^2 + \left(1+\kappa_3\kappa_4\right)s_i + \left(2\kappa_4 + J_i\kappa_3\right) = 0, i = 1,2,3. \tag{43}$$

The parameter selection criteria is that all the solutions to (43) have negative real parts. Next, as a prior selection of the position controller parameter, κ_{2z} can be determined by first considering the nonsingular condition $\kappa_{2z} < (g - \overline{a}_0 - \overline{u} - \Delta\overline{u})/2$ as well as desired trajectory, fault recoverability and robust capability. By linearizing the closed-loop error position system around equilibrium $\widetilde{p} = \widetilde{v} = 0$

$$\dot{\widetilde{v}} = -K_1K_2\widetilde{p} - 2K_2\widetilde{v}, \tag{44}$$

we have its characteristic polynominal

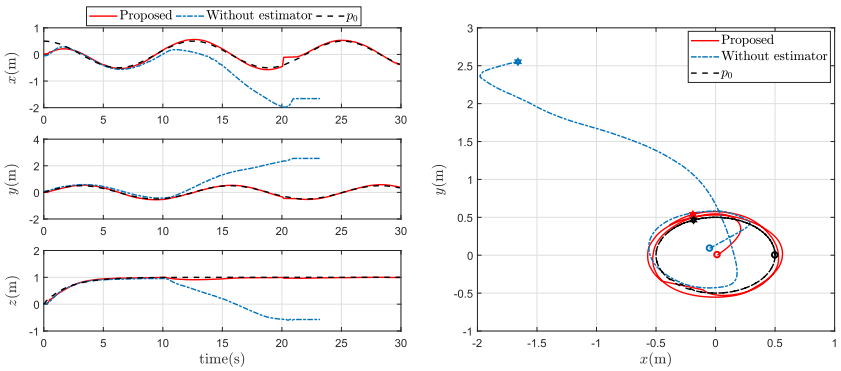

(a) Position in each axis (b) Horizonal trajectory

Fig. 9. Position of quadrotor in Case I. (∘ represents the initial position and * represents the final position.).

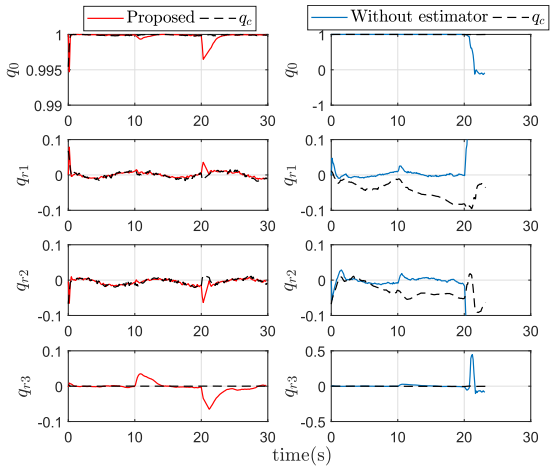

Fig. 10. Attitude of quadrotor in Case I.

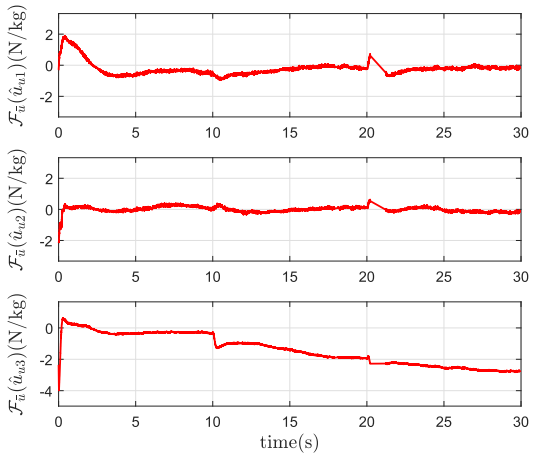

Fig. 11. Estimate in position loop in Case I.

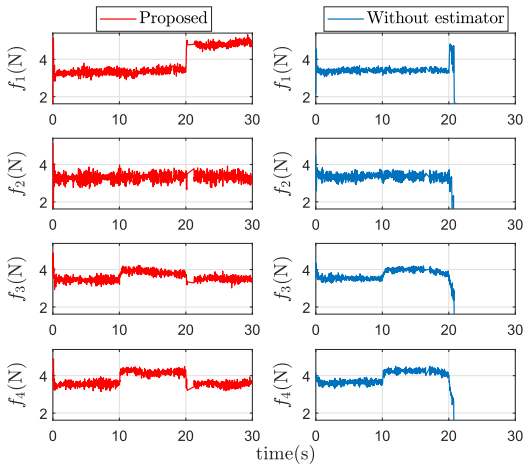

Fig. 12. Control command of each rotor in Case I.

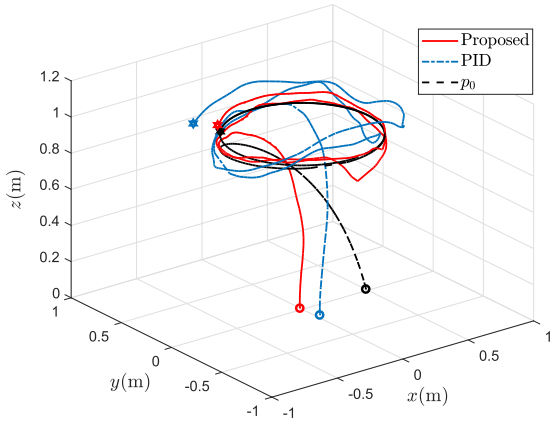

Fig. 13. Trajectory of quadrotor in Case II. (∘ represents the initial position and * represents the final position.).

$$s_i^2 + 2\kappa_{2i}s_i + \kappa_{1i}\kappa_{2i} = 0, i = x, y, z. \tag{45}$$

By choosing κ_{1i} and κ_{2i} such that all the solutions to (45) have negative real parts. Then, based on this principle and the parameters from numerical simulations, the nominal controller can be implemented after a satisfied performance is obtained by trail and error. Besides, simple tuning of estimator parameters can be obtained due to the fact that there is merely a single parameter involved. Small filter parameter could contribute to high estimate accuracy but possible control chattering since it is introduced as the denominator in the estimator. An initial choice can be made by using the value in the numerical simulation. Then, after simple tuning by increasing the filter parameter, a good performance can be obtained when the UAV does not show any chattering phenomenon.

6.2. Experimental results

6.2.1. Case I. The proposed strategy vs nonsingular strategy

To highlight the robustness and fault tolerant capability of the proposed control strategy, comparison experiment is also implemented by the nonsingular strategy without dynamics estimator. The desired trajectory is assigned as $p_0 = [0.5\cos(0.5t), 0.5\sin(0.5t), 1 - e^{-0.5t}]^T m$. The fault coefficient of each propeller is injected based on Table 3. The control parameters of the proposed strategy are chosen as $K_1 = 4I_3, K_2 = \mathrm{diag}(0.1, 0.1, 0.15), \kappa_3 = 7, \kappa_4 = 5, \alpha_p = 4, \alpha_a = 0.2, \overline{u} = 5$, and $\Delta\overline{u} = 0.1$. Experimental results of the quadrotor trajectory tracking under propeller fault are presented in Figs. 8–12.

An overall description of the trajectory tracking under different controllers is summarized in Fig. 8. The position and horizonal trajectory of the quadrotor are shown in Fig. 9. It can be observed that the tracking operation is achieved by the proposed strategy with a good performance while the mission is failed without dynamics estimator after the fault is injected. Despite of the transient response after the propeller fault occurs, the high performance trajectory tracking can be recovered quickly by the proposed strategy. Moreover, it can be seen from Fig. 10 that the proposed strategy achieves a better attitude tracking. The output of the dynamics estimator in position loop is drawn in Fig. 11. The control commands of propellers are collected in Fig. 12. It can be observed that all the signals

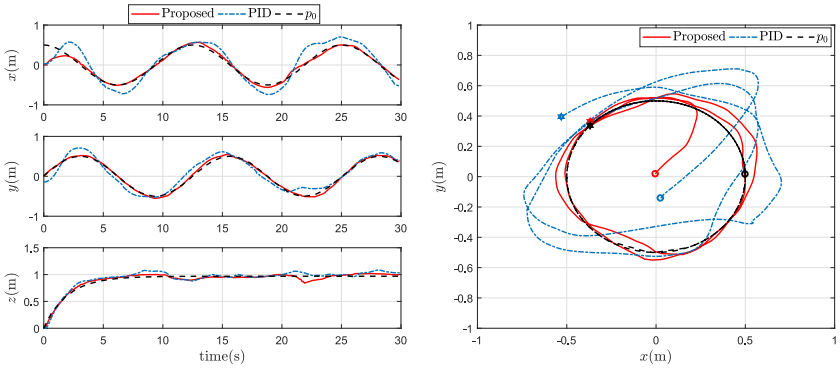

(a) Position in each axis (b) Horizonal trajectory

Fig. 14. Position of quadrotor in Case II. (∘represents the initial position and * represents the final position.).

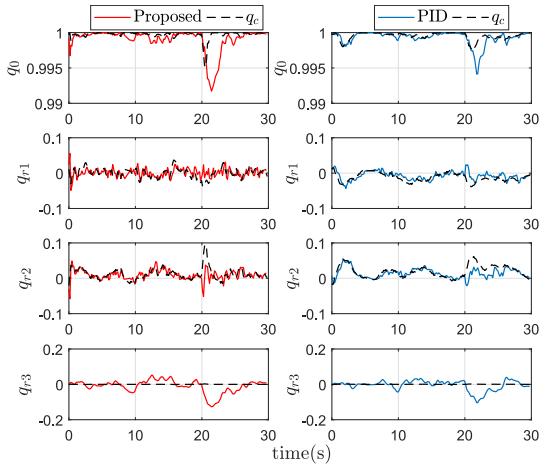

Fig. 15. Attitude of quadrotor in Case II.

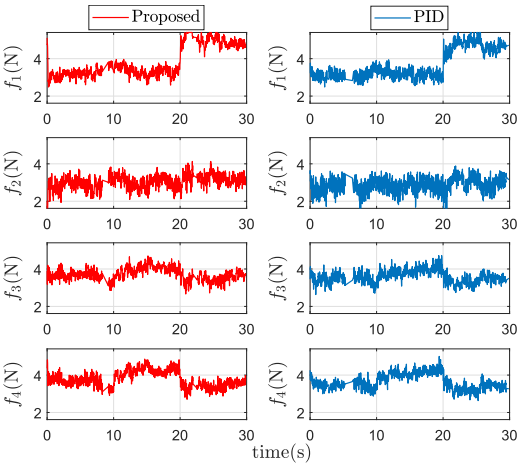

Fig. 16. Control command of each rotor in Case II.

Table 5
Fault Coefficient of Example 1 in Case III.

	$0 \leqslant t < 10$s	$10\text{s} \leqslant t < 20$s	$t \geqslant 20$s
v_1	0	0	Example 1: 35%(Example 2: 30%)
v_2	0	0	Example 1: 0(Example 2: 15%)
v_3	0	10%	0
v_4	0	15%	0

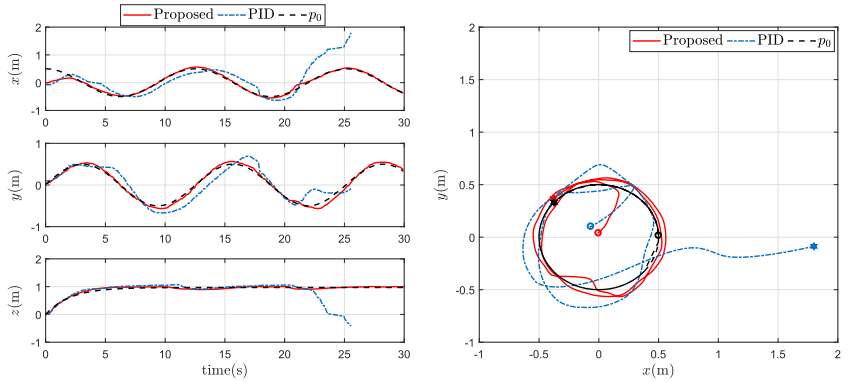

(a) Position in each axis (b) Horizonal trajectory

Fig. 17. Position of quadrotor of Example 1 in Case III. (◦represents the initial position and * represents the final position.).

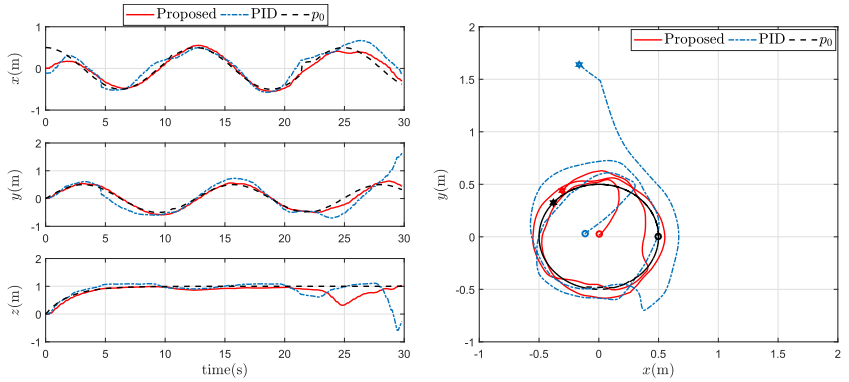

(a) Position in each axis (b) Horizonal trajectory

Fig. 18. Position of quadrotor of Example 2 in Case III. (◦represents the initial position and * represents the final position.).

remain bounded and the dynamics estimator could provide the fault compensation for the control command of the faulty propeller. Without any compensation mechanism, the nonsingular strategy fails to complete the trajectory tracking.

6.2.2. Case II. The proposed strategy vs PID control: comparison 1

In this case, the tracking performance of the quadrotor simultaneously subject to propeller fault and wind disturbance is presented, where a well-tuned PID controller is also implemented for comparison experiment. The control parameters of the proposed strategy, propeller fault and desired trajectory are chosen as the same as that in Case I. The parameters of the PID controller for position loop are selected as $K_{P1} = \text{diag}(0.95, 0.95, 1), K_{P2} = \text{diag}(0.09, 0.09, 0.2), K_I = \text{diag}(0.02, 0.02, 0.05)$ and $K_D = \text{diag}(0.01, 0.01, 0)$, and for the attitude loop are $K_{P1} = 7I_3, K_{P2} = 0.15I_3, K_I = 0.05I_3$ and $K_D = 0.003I_3$. Moreover, a large electrical fan is employed to generate the persistent wind with a 4 m/s velocity with respect to the trajectory center. Figs. 13–16 summarize the experimental results under propeller fault and wind disturbance.

Fig. 13 describes the trajectories of the quadrotor driven by the proposed and PID controllers. Fig. 14 draws the position and the horizonal trajectory. Fig. 15 compares the attitude tracking performance by showing the time history of the quaternion. It can be observed that the proposed strategy ensures a better tracking performance despite of the propeller fault and persistent wind disturbance. Table 2 collects the mean deviation (MD), standard deviation (SD), convergence time (CT) and energy consumption (EC) of the

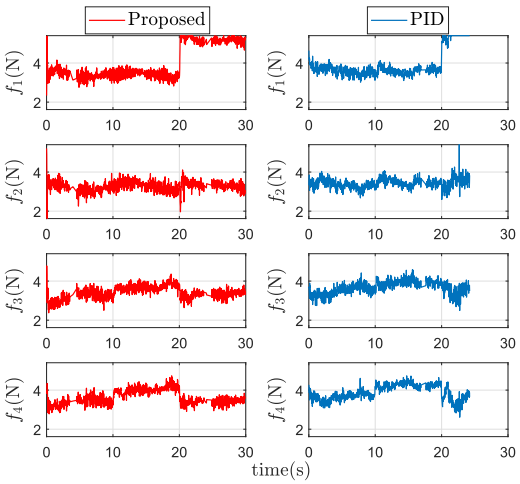

Fig. 19. Control command of each rotor of Example 1 in Case III.

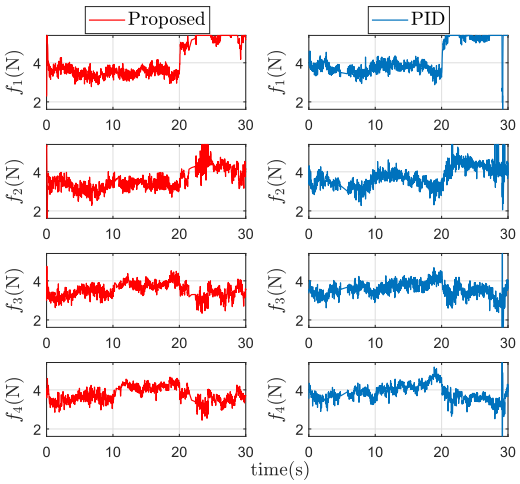

Fig. 20. Control command of each rotor of Example 2 in Case III.

Table 6
Tracking performance comparison of the proposed strategy in Case III.

Eample	MD, m	SD, m	CT, s	EC, Ns
1	0.0073	0.1202	3	7.2353
2	0.0141	0.2361	3	7.5490

trajectory tracking during the experiment, where EC is calculated by using $\sum_{i=1}^{4}\int_0^T f_i(t)\mathrm{d}t/T$. It can be calculated from Table 2 that, in contrast to the PID controller, the proposed strategy can achieve the tracking by improving the MDE and STDE by 69.00% and 68.83% with merely 4.16% additional energy consumption. This further indicates that the proposed strategy achieves a higher tracking accuracy. It can be seen from the control commands in Fig. 16 that the dynamics estimator also works well to provide robust compensation under wind disturbance. Therefore, it can be concluded from experimental results that the proposed strategy achieves the trajectory tracking of the quadrotor with a better performance than the PID controller while showing a better robustness to the propeller fault and harsh wind condition.

6.2.3. Case III. The proposed strategy vs PID control: comparison 2

In this case, two examples are conducted by the proposed strategy and PID control in the same experimental scenario. To show the advantage, more serious fault conditions are introduced. The fault coefficients of Examples 1 and 2 are injected based on Table 5, respectively. The persistent wind with a 4 m/s velocity with respect to the trajectory center is also employed.

It can be observed from Figs. 17 and 18 that the proposed strategy achieves both trajectory tracking scenarios and the PID control fails to provide the suitable compensation when larger fault occurs at 20s. Figs. 19 and 20 present the command control signal of each rotor in each Example. It can be seen that the saturation phenomena appear in rotor 1 when the faults are injected at 20s. The PID control strategy fails in this case is because of that the rotors can not provide enough control force and torque to compensate for the desired acceleration. Despite of the fact that the proposed control strategy completes the trajectory tracking in this case, however, it also fails when we rise the fault up to 45% of rotor 1. This implies that the trajectory tracking may not be achieved if the faulty rotor can not generate enough control. Besides, the quantitative evaluation is also summarized in Table 6 that shows a good performance in the presence of serious propeller fault and harsh wind condition.

7. Conclusion

In this paper, we propose a robust passive fault-tolerant control strategy for the trajectory tracking of the VTOL UAV subject to partial propeller fault and external disturbance. A force command and a torque command are exploited for the position and attitude loops tracking, respectively. To compensate for the system uncertainties, a first-order filter based dynamics estimator is employed. A novel smooth saturation function is introduced in the force command to guarantee its boundedness and differentiability. The ultimate boundedness of the overall closed-loop system is proved. In addition, the explicit and simple selection criteria of control gains and estimator parameters are analyzed. Simulation and experiment results with comparison examples demonstrate that the proposed strategy achieves the trajectory tracking of the quadrotor and guarantees the robustness to propeller fault and wind disturbance.

Declaration of Competing Interest

The authors declare that they have no known competing financial interests or personal relationships that could have appeared to influence the work reported in this paper.

Acknowledgments

This work was supported in part by Development of Drone System for Ship and Marine Mission (2.210065.01) of Institute of Civil-Military Technology Cooperation, the National Research Foundation of Korea (NRF) grant funded by the Korea government (MSIT) (No. 2020R1F1A1075857), Basic Science Research Program through the National Research Foundation of Korea (NRF) funded by the Ministry of Education (No. 2020R1A6A1A03040570), and Research on Algorithm of Autonomous Operation for Heterogeneous Multiple Small UAVs funded by Agency for Defense Development (LIGNEX1-2020-0528(00)), respectively.

Appendix A. Supplementary data

Supplementary data associated with this article can be found, in the online version, athttps://doi.org/10.1016/j.ymssp.2021.108062.

References

[1] H. Shraim, A. Awada, R. Youness, A survey on quadrotors: configurations, modeling and identification, control, collision avoidance, fault diagnosis and tolerant control, IEEE Aerospace Electron. Syst. Mag. 33 (7) (2018) 14–33.
[2] Y. Zou, Z. Meng, Coordinated trajectory tracking of multiple vertical take-off and landing UAVs, Automatica 99 (2019) 33–40.
[3] A. Abdessameud, A. Tayebi, Global trajectory tracking control of VTOL-UAVs without linear velocity measurements, Automatica 46 (6) (2010) 1053–1059.
[4] K. Xia, S. Lee, H. Son, Adaptive control for multi-rotor UAVs autonomous ship landing with mission planning, Aerospace Sci. Technol. 96 (2020), 105549.
[5] B. Zhu, W. Huo, Nonlinear control for a model-scaled helicopter with constraints on rotor thrust and fuselage attitude, Acta Autom. Sin. 40 (11) (2014) 2654–2664.
[6] Y. Zou, Z. Zheng, A robust adaptive RBFNN augmenting backstepping control approach for a model-scaled helicopter, IEEE Trans. Control Syst. Technol. 23 (6) (2015) 2344–2352.
[7] Z. Zuo, P. Ru, Augmented L1 adaptive tracking control of quad-rotor unmanned aircrafts, IEEE Trans. Aerospace Electron. Syst. 50 (4) (2014) 3090–3101.
[8] B. Zhao, B. Xian, Y. Zhang, X. Zhang, Nonlinear robust sliding mode control of a quadrotor unmanned aerial vehicle based on immersion and invariance method, Int. J. Robust Nonlinear Control 25 (2015) 3714–3731.
[9] D. Cabecinhas, R. Cunha, C. Silvestre, A nonlinear quadrotor trajectory tracking controller with disturbance rejection, Control Eng. Practice 26 (2014) 1–10.
[10] H. Liu, D. Li, Z. Zuo, Y. Zhong, Robust three-loop trajectory tracking control for quadrotors with multiple uncertainties, IEEE Trans. Ind. Electron. 63 (4) (2016) 2263–2274.
[11] K. Guo, J. Jia, X. Yu, L. Guo, L. Xie, Multiple observers based anti-disturbance control for a quadrotor UAV against payload and wind disturbances, Control Eng. Practice 102 (2020), 104560.
[12] X. Shao, J. Liu, H. Wang, Robust back-stepping output feedback trajectory tracking for quadrotors via extended state observer and sigmoid tracking differentiator, Mech. Syst. Signal Process. 104 (2018) 631–647.
[13] M. He, J. He, S. Scherer, Model-based real-time robust controller for a small helicopter, Mech. Syst. Signal Process. 146 (2021), 107022.
[14] Y. Huang, M. Zhu, Z. Zheng, Output-constrained fixed-time control for autonomous ship landing of helicopters, ISA Trans. 106 (2020) 221–232.
[15] B. Wang, Y. Shen, Y. Zhang, Active fault-tolerant control for a quadrotor helicopter against actuator faults and model uncertainties, Aerospace Sci. Technol. 99 (2020), 105745.
[16] B. Xian, W. Hao, Nonlinear robust fault-tolerant control of the tilt trirotor UAV under rear servo's stuck fault: Theory and experiments, IEEE Trans. Ind. Inf. 15 (4) (2018) 2158–2166.

[17] R.C. Avram, X. Zhang, J. Muse, Nonlinear adaptive fault-tolerant quadrotor altitude and attitude tracking with multiple actuator faults, IEEE Trans. Control Syst. Technol. 26 (2) (2018) 701–707.
[18] B. Wang, X. Yu, L. Mu, Y. Zhang, Disturbance observer-based adaptive fault-tolerant control for a quadrotor helicopter subject to parametric uncertainties and external disturbances, Mech. Syst. Signal Process. 120 (2019) 727–743.
[19] F. Chen, R. Jiang, K. Zhang, B. Jiang, G. Tao, Robust backstepping sliding-mode control and observer-based fault estimation for a quadrotor UAV, IEEE Trans. Ind. Electron. 63 (8) (2016) 5044–5056.
[20] R.C. Avram, X. Zhang, J. Muse, Quadrotor actuator fault diagnosis and accommodation using nonlinear adaptive estimators, IEEE Trans. Control Syst. Technol. 25 (6) (2017) 2219–2226.
[21] H.J. Ma, Y. Liu, T. Li, G.H. Yang, Nonlinear high-gain observer-based diagnosis and compensation for actuator and sensor faults in a quadrotor unmanned aerial vehicle, IEEE Trans. Ind. Inf. 15 (1) (2019) 550–562.
[22] X. Wang, E.J. van Kampen, Q. Chu, Quadrotor fault-tolerant incremental nonsingular terminal sliding mode control, Aerospace Sci. Technol. 95 (2019), 105514.
[23] Y. Song, L. He, D. Zhang, J. Qian, J. Fu, Neuroadaptive fault-tolerant control of quadrotor UAVs: a more affordable solution, IEEE Trans. Neural Netw. Learn. Syst. 30 (7) (2019) 1975–1983.
[24] X. Zhang, T. Parisini, M.M. Polycarpou, Adaptive fault-tolerant control of nonlinear uncertain systems: an information-based diagnostic approach, IEEE Trans. Autom. Control 49 (8) (2004) 1259–1274.
[25] Y. Zou, K. Xia, Robust fault-tolerant control for under-actuated takeoff and landing UAVs, IEEE Trans. Aerospace Electron. Syst. 56 (5) (2020) 3545–3555.
[26] Y. Zou, Singularity-free adaptive fault-tolerant trajectory tracking controller for VTOL UAVs, Int. J. Syst. Sci. 48 (10) (2017) 2223–2234.
[27] A.R. Merheb, H. Noura, F. Bateman, Emergency control of AR drone quadrotor UAV suffering a total loss of one rotor, IEEE/ASME Trans. Mechatron. 22 (2) (2017) 961–971.
[28] W. Chung, H. Son, Fault-tolerant control of multirotor UAVs by control variable elimination, IEEE/ASME Trans. Mechatron. 25 (5) (2020) 2513–2522.
[29] J. Na, A.S. Chen, Y. Huang, et al., Air-fuel ratio control of spark ignition engines with unknown system dynamics estimator: theory and experiments, IEEE Trans. Control Syst. Technol. 29 (2) (2021) 786–793.
[30] S. Wang, L. Tao, Q. Chen, J. Na, X. Ren, USDE-based sliding mode control for servo mechanisms with unknown system dynamics, IEEE/ASME Trans. Mechatron. 25 (2) (2020) 1056–1066.
[31] M.D. Shuster, A survey of attitude representations, J. Astronaut. Sci. 41 (4) (1993) 439–517.
[32] T. Chen, M. Zhu, Z. Zheng, Asymmetric error-constrained path-following control of a stratospheric airship with disturbances and actuator saturation, Mech. Syst. Signal Process. 119 (2019) 501–522.
[33] A. Castillo, R. Sanz, P. Garcia, W. Qiu, H. Wang, C. Xu, Disturbance observer-based quadrotor attitude tracking control for aggressive maneuvers, Control Eng. Practice 82 (2019) 14–23.
[34] K. Xia, H. Son, Adaptive fixed-time control of autonomous VTOL UAVs for ship landing operations, J. Franklin Inst. 357 (2020) 6175–6196.